Climate Dynamics (2000) 16: 333–354

C. Frankignoul · E. Kestenare · N. Sennéchael
G. de Coëtlogon · F. D'Andrea

On decadal-scale ocean-atmosphere interactions in the extended ECHAM1/LSG climate simulation

Received: 2 April 1999 / Accepted: 14 October 1999

Abstract The last 810 years of a control integration with the ECHAM1/LSG coupled model are used to clarify the nature of the ocean-atmosphere interactions at low frequencies in the North Atlantic and the North Pacific. To a first approximation, the atmosphere acts as a white noise forcing and the ocean responds as a passive integrator. The sea surface temperature (SST) variability primarily results from short time scale fluctuations in surface heat exchanges and Ekman currents, and the former also damp the SST anomalies after they are generated. The thermocline variability is primarily driven by Ekman pumping. Because the heat, momentum, and vorticity fluxes at the sea surface are correlated in space and time, the SST variability is directly linked to that in the ocean interior. The SST is also modulated by the wind-driven geostrophic fluctuations, resulting in persistent correlation with the thermocline changes and a slight low-frequency redness of the SST spectra. The main dynamics are similar in the two oceans, although in the North Pacific the SST variability is more strongly influenced by advection changes and the oceanic time scales are larger. A maximum covariance analysis based on singular value decomposition in lead and lag conditions indicates that some of the main modes of atmospheric variability in the two oceans are sustained by a very weak positive feedback between the atmosphere, SST, and the strength of the subtropical and subpolar gyres. In addition, in the North Atlantic the main surface pressure mode has a small quasi-oscillatory component at 6-year period, and advective resonance occurs for SST around 10-year period, both periods being also singled out by multichannel singular spectrum analysis. The ocean-atmosphere coupling is however much too weak to redden the tropospheric spectra or create anything more than tiny spectral peaks, so that the atmospheric and oceanic variability is dominated in both ocean sectors by the one-way interactions.

C. Frankignoul (✉) · E. Kestenare · N. Sennéchael
G. de Coëtlogon
Laboratoire d'Océanographie Dynamique et de Climatologie,
Unité mixte de recherche CNRS-ORSTOM-UPMC,
Université Pierre et Marie Curie, Case 100, 4 place Jussieu,
75252 Paris Cedex 05, France
E-mail: cf@lodyc.jussieu.fr

F. D'Andrea
Laboratoire de Météorologie Dynamique,
Ecole Normale Supérieure, 24, rue Lhomond,
75231 Paris Cedex 05, France

1 Introduction

The decadal variability in the first few hundred years of the ECHAM1/LSG coupled simulation has been investigated in the North Pacific by von Storch (1994) and Robertson (1996), and in the North Atlantic by Zorita and Frankignoul (1997). Using multichannel singular spectrum analysis (MSSA), also called extended empirical orthogonal function (extended EOF) analysis, Robertson (1996) found that the SST spectrum was predominantly red in the North Pacific and had a significant peak with an 18 year period that was associated with an irregular, primarily standing oscillation of the ocean-atmosphere system where the SST changes were largely driven by anomalous advection. Robertson suggested that the North Pacific mode beared similarity with that discussed by Latif and Barnett (1994) in the ECHO coupled model and might be maintained by a positive midlatitude ocean-atmosphere feedback involving changes in the gyre strength. On the other hand, Zorita and Frankignoul (1997 hereafter ZF) found no spectral peak in the North Atlantic, the spectrum of SST being primarily white at low frequencies, compared to red in the ocean interior. Extended EOF analysis detected a 20 and a 10-year mode of ocean-atmosphere variability which primarily reflected the oceanic response to the atmospheric forcing, although there was a hint of

an active oceanic role in the 10-year mode since it was detected in the atmosphere alone, albeit with much difficulty.

Whether or not these differences in decadal behavior between the North Atlantic and the North Pacific reflect different air-sea interactions needs to be established. Other coupled model analysis show no major differences between the two oceans at the decadal scale, both playing an active role in ECHO (Latif and Barnett 1994; Grötzner et al. 1998) and a passive one in the GFDL model (Delworth 1996). However, these analyses were made in a similar way for the two oceans while the ECHAM1/LSG results were obtained using different methods, that is Robertson (1996) band-pass filtered prior to using MSSA, while ZF filtered little and also relied on lagged correlation. MSSA is a very efficient method for detecting cyclical behaviors but often overemphasizes their relative importance and may confuse them with colored noise (Allen and Smith 1996), in particular when there is propagation occuring. In addition, MSSA is of little use in establishing causal relations because it acts as a strong narrow-band pass filter and only describes the simultaneous behavior of different variables.

We focus on the last 810 years of the ECHAM1/LSG run when the model has reached a statistically steady state, and study the decadal variability with statistical methods that distinguish more adequately between cause and effect, using unfiltered yearly averaged data. By analyzing the two ocean sectors in the same fashion, we show that there is no obvious difference in their behavior, except for longer time scales in the North Pacific. The ocean responds primarily passively to the atmosphere, but in both cases there is also evidence of some active coupling, albeit very weak. The coupled model is described in Sect. 2. The North Atlantic variability is investigated in Sect. 3, the North Pacific one in Sect. 4, and the results are discussed in Sect. 5.

2 Model description

The climate model used in this study is the ECHAM1/LSG coupled GCM developed at the Max-Planck-Institut für Meteorologie in Hamburg and described by Cubasch et al. (1992) and von Storch et al. (1997). The atmospheric component is the spectral ECHAM1-T21 model with 19 levels (Roeckner et al. 1992). Prognostic variables are vorticity, divergence, temperature, surface pressure, water vapor and cloud water; soil processes are parametrized. The ocean component is the Large-Scale-Geostrophic (LSG) model (Maier-Reimer et al. 1993) with an effective resolution of about $4° \times 4°$ and 11 vertical levels, the first 5 being located at 25 m, 75 m, 150 m, 250 m, and 450 m, and a smoothed topography. In this primitive equation model, the non-linear advection of momentum is neglected and fast gravity waves strongly damped by an implicit integration scheme. An explicit horizontal diffusion of $2\,10^2\ m^2\ s^{-1}$ and viscosity of $5\,10^4\,m^2\ s^{-1}$ counteract the inherent tendency for mode splitting in the model E grid. A convective mixing scheme is applied whenever the stratification becomes unstable. Sea ice simply appears when the water temperature falls below the freezing point. The atmospheric and oceanic components are coupled synchronously, but the basic ocean time step of 30 days is reduced to 1 day for the computation of temperature, salinity, and sea ice in the first two ocean levels in order to resolve the upper ocean response to the synoptic variability of the atmosphere. A large flux correction (given in Gates et al. 1993) is applied to reduce climate drift.

As discussed by von Storch et al. (1997), the coupled model was not in equilibrium at the beginning of the integration because of an imbalance in the oceanic heat and freshwater fluxes linked to the applied flux correction, resulting in very large changes in the sea-ice cover. However, after year 450 a quasi-stationary state was reached, although the globally integrated freshwater flux remained unbalanced, due to the changes in the snow accumulation rate over Greenland and Antarctica which induced a linear increase in the salinity of the upper ocean. There was also a small increase of temperature and salinity below 1000 m which created a very slight increase in the strength of the thermohaline circulation. Thus, we focus our analysis over the last 810 years of the 1260-year integration, removing by least-squares fit a quadratic trend from each variable. The mean atmospheric circulation in the Northern Hemisphere is well-reproduced in summer but has some unrealistic features in winter: the Aleutian low is too deep, the sea level pressure over the Arctic too high, and the Icelandic low underestimated and shifted about 20° too far south, so that the westerlies over the North Atlantic are maximum around 35°–40°N and the gyre system is shifted southward. Because of the strong heat flux correction, however, the mean SST is realistic. The gross features of the ocean circulation are rather well-reproduced, except near the equator where the ocean dynamics are poorly represented. Because of the low-resolution, the western boundary currents are broad and weak.

To emphasize the low frequency ocean-atmosphere interactions at the basin scale, we considered separately the North Atlantic and the North Pacific regions, limiting our analysis to the 4°–67°N domain, using yearly averaged data with no additional smoothing. As discussed by Sennéchael et al. (in preparation), the higher latitudes in the North Atlantic and the salinity field play a role in the mean overturning circulation, but have little influence on the midlatitude variability discussed here.

3 The North Atlantic variability

3.1 Main patterns of variability

The dominant patterns of atmospheric variability are equivalent barotropic and have a large zonal scale, as illustrated in Fig. 1 by the first two EOFs (estimated without area weighting, which has little influence on the results) of the yearly surface pressure (top) and curl τ/f (bottom), which is proportional to the Ekman pumping. The higher EOFs have smaller scales and substantially less variance. The EOF time series (or principal components, hereafter PCs) of each of the two variables are uncorrelated at all lags, suggesting primarily standing fluctuations. However, the PCs of surface pressure are correlated at zero lag with those of curl τ/f, most notably PC1 of surface pressure and PC2 of curl τ/f (correlation coefficient $r = 0.8$), and PC2 of surface pressure and PC1 of curl τ/f ($r = -0.7$). The former pair of patterns describes a meridional shift of the westerlies, while the latter primarily corresponds to their strengthening or weakening and can be considered to best correspond to the North Atlantic Oscillation, even though it is shifted south in the model. The yearly PCs have negligible persistence and primarily behave like white noise (Fig. 2, top). A close inspection reveals small spectral peaks, but they are only (marginally) significant near 6-year period

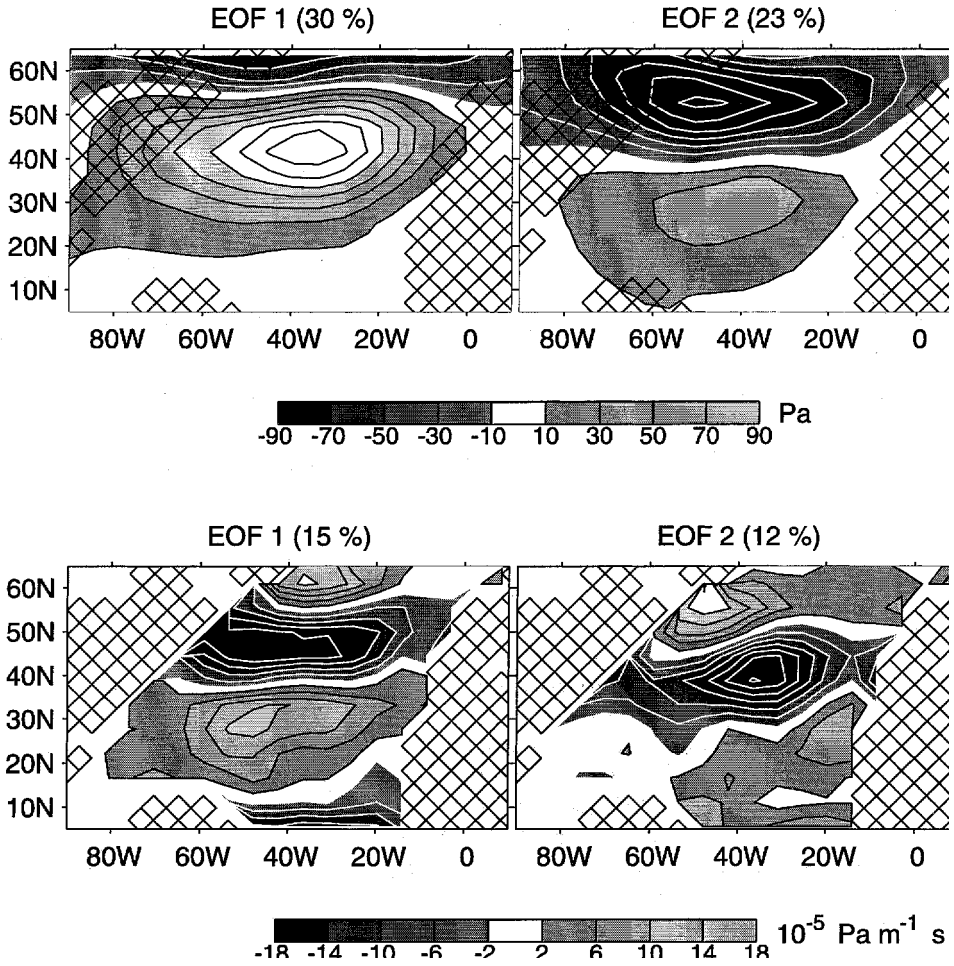

Fig. 1 First two EOFs of the yearly anomalies in surface pressure (in Pa, *top*) and curl τ/f (in 10^{-5} Pa m^{-1} s, *bottom*) in the North Atlantic region. The EOFs indicate typical amplitudes as the PCs are normalized. Positive (negative) isolines are in *black* (*white*). The EOF *number* and *fractional variance* are shown in the figure title

for PC1 of surface pressure and both PCs of curl τ/f. All frequency spectra were calculated with the multi-taper method using a window length of 810 year and 9 Slepian tapers ($NW = 5$), which is appropriate to their limited redness (Percival and Walden 1993). Statistical significance at the 5% level was verified by considering each half of the series separately and reducing the number of tapers ($NW = 4$). Correspondingly, these PCs show a slight negative auto-correlation at lag 3 which is significant at the 5% level only for PC2 of curl τ/f (Fig. 3). It is suggested below that these minor departures from white noise result from an oscillatory behavior, albeit with very little variance. Figure 4 (top) represents the first two EOFs of the yearly SST anomalies, which are rather similar but for a northeastward shift. As PC1 is weakly correlated positively with PC2 when PC1 leads by 1 year and negatively when it lags by 3 years, the dominant SST patterns tend to propagate slowly northeastward, consistently with the mean near-surface circulation (Fig. 5). The SST PCs have an e-folding scale of 1 or 2 years (Fig. 3), and their frequency spectrum is white at low frequencies, approximately decaying as $\omega^{-1/2}$ (ω is frequency) for periods shorter than decadal, without statistically significant peak (Fig. 2, bottom left).

As illustrated in Fig. 3 (right), a cross-correlation with the atmospheric PCs shows that there is no correlation when SST leads the atmosphere, the correlations are large when the two media are in phase, and they decay like the SST PCs when the ocean follows. Frankignoul and Hasselmann (1977) have shown that it is the statistical signature of a passive oceanic response to white noise atmospheric forcing if the interaction can be approximated as a first order autoregressive process. A sign reversal between lead and lag conditions would be characteristic of a negative atmospheric feedback, as the atmosphere would damp the SST fluctuations it had generated, while for positive feedback the correlation would remain of one sign, being largest when the ocean follows (Frankignoul et al. 1998). This also applies to correlation or covariance maps and will be used repeatedly in the following, but note that it requires that the atmospheric forcing is white at low frequencies. The lag of maximum correlation depends on the relative value of the oceanic decay time and the length of data averaging: here it occurs at lag 0 because the data are averaged over a duration larger than the SST decay time, but it occurs at lag 1 if monthly data are used (see ZF).

To represent the variability in the oceanic thermocline, we use the baroclinic pressure at 250 m (hereafter p_{bc}), which is related to thermocline displacement and reflects the main interior dynamics, as discussed by Frankignoul et al. (1997, hereafter FMZ). It was esti-

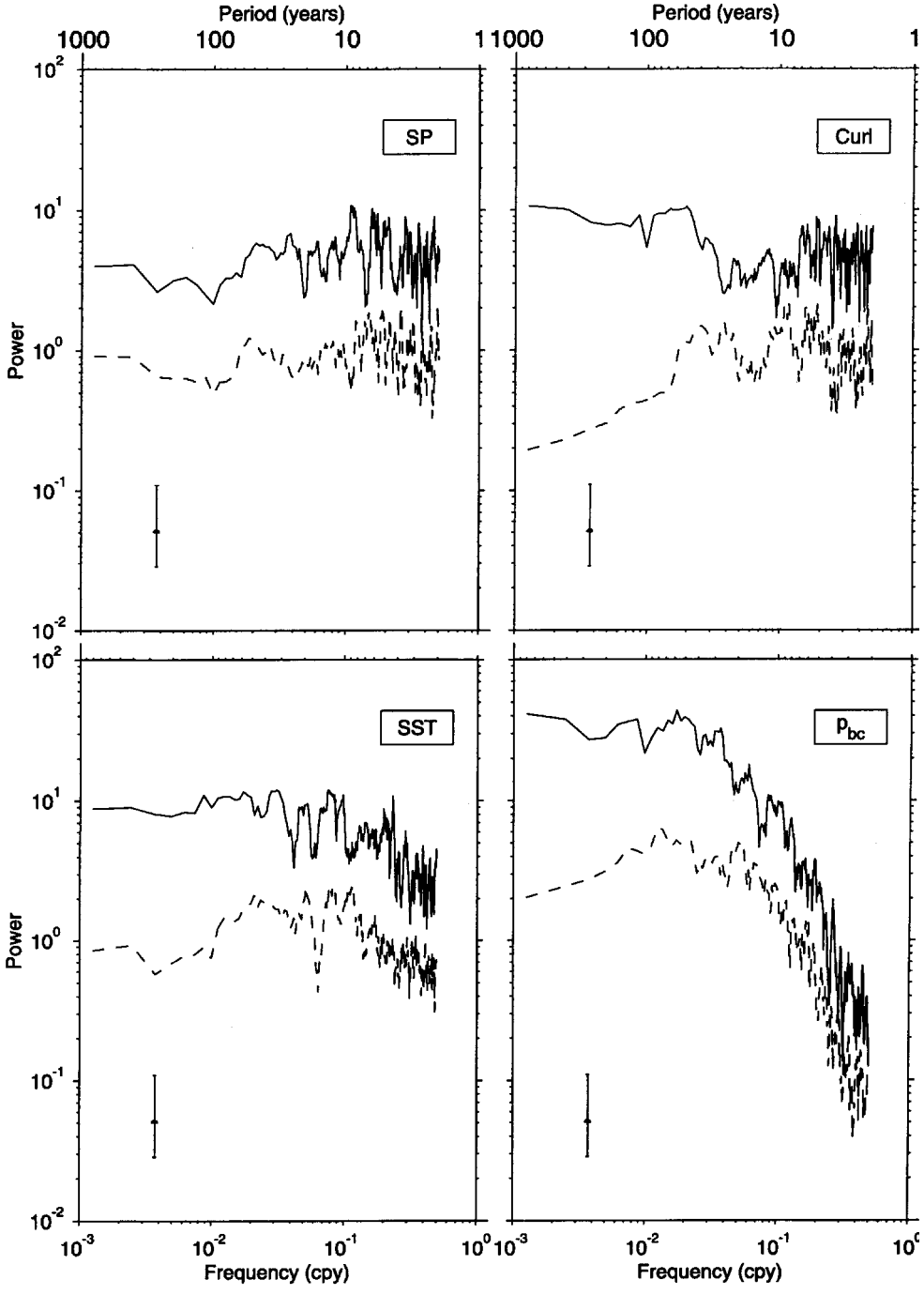

Fig. 2 Multitaper spectrum of the first (*solid line*) and second (*dashed line*) PC of surface pressure (*top left*), curl τ/f (*top right*), SST (*bottom left*), and p_{bc} (*bottom right*) in the North Atlantic. The spectra of the first PCs are shifted upward by a factor 5, and the error bars give the 95% confidence interval

mated by least squares fit from the baroclinic currents and is thus defined on a smaller domain than the SST. The first EOF is a dipole which describes in-phase changes in the intensity of the model subtropical and subpolar gyres while the second EOF mainly indicates a meridional shift in gyre separation (Fig. 4, bottom). Both modes have a persistence of several years (Fig. 3, left) and a red spectrum, with a longer dominant time scale for PC1 (Fig. 2). Again, no statistically significant spectral peak could be detected. The main PCs are correlated at various non-zero lags, corresponding in particular to westward propagation south of 35°N, which is seen in Fig. 6. Cross-correlation with the atmospheric PCs shows that the thermocline variability is driven by the atmosphere, with maximum correlation when p_{bc} lags the Ekman pumping by 1 year since its characteristic time exceeds the length of data averaging (Fig. 3, right). Note that the difference in response time between SST and p_{bc} results in SST leading p_{bc} by 1 year. This explains why SST leads the Gulf Stream transport in Grötzner et al. 1998. Using the first 325 years of the run, FMZ have shown that the thermocline variability south of 35°N was consistent with a linear, baroclinic response to Ekman pumping, which act as a white noise

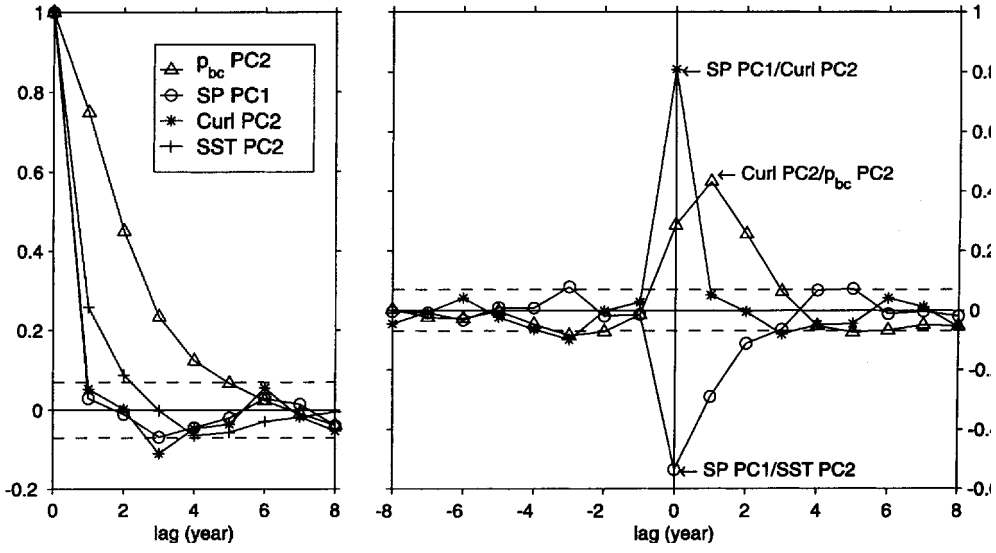

Fig. 3 Auto-correlation of PC1 of surface pressure, PC2 of curl τ/f, PC2 of SST, and PC2 of p_{bc} (*left*). Cross-correlation (*right*) between PC1 of surface pressure and PC2 of SST (*circle*), and between PC2 of curl τ/f and PC2 of p_{bc} (*triangle*); ocean leads at negative lags. Cross-correlation (*right*) between PC1 of surface pressure and PC2 of curl τ/f (*star*); curl τ/f leads at negative lags. The *dashed line* indicates the 5% level for zero correlation

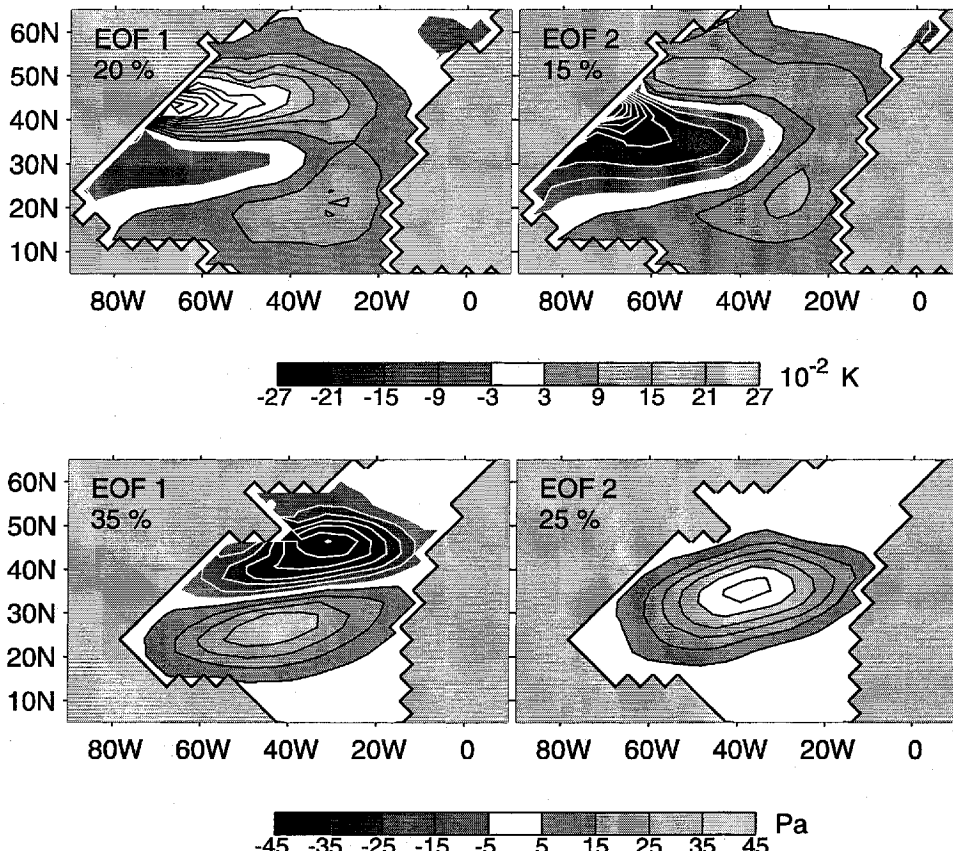

Fig. 4 As in Fig. 1 for the first two EOFs of SST (*top*, in 10^{-2} K) and baroclinic pressure at 250 m (*bottom*, in Pa)

forcing. The variance (not the spectrum) has a weak maximum near the decadal period which is linked to the travel time of a first mode baroclinic Rossby wave across the basin, and the spectral flattening at very low frequencies reflects baroclinic adjustment.

There are strong and persistent correlations between the SST and p_{bc} PCs in lead and lag conditions, but no single one-to-one correspondence: each p_{bc} PC somewhat correlates with each SST PC, with maxima found at lag 0, 1, or −1, depending on the particular pair. As documented later, this results from the interplay between the correlated forcing of the two variables by the atmospheric variability and the SST modulation by the geostrophic fluctuations, with the differences in persistence and propagation of the two fields adding to the complexity.

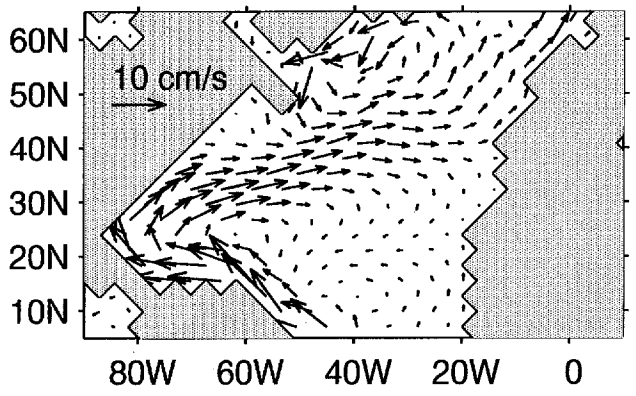

Fig. 5 Mean horizontal current in the upper two layers of the North Atlantic

3.2 Correlation analysis

Using the main PCs of SST or p_{bc} as a basis for understanding the links between ocean and atmosphere leads to ambiguous interpretation because they are strongly auto- and cross-correlated (except at zero lag, by definition). Hence, the lagged correlation of an atmospheric variable with an oceanic PC may reflect its unlagged correlation with another. On the other hand, since the yearly PCs of surface pressure or curl τ/f are neither auto-correlated (except very weakly at lag 3, as discussed above) nor cross-correlated, they form an ideal basis to investigate the lead and lag relations between the two media.

To illustrate how the atmosphere forces the ocean, we choose the Ekman pumping PC1 as our basis time series. Since it is white, the 5% confidence level is 0.07 (0.06) for a two-sided (one-sided) test. Statistical significance was verified by considering separately the two halves of the 810-year run. The correlation maps of curl τ/f PC1 with p_{bc}, surface current, SST, and net surface heat flux into the ocean for lags between −1 year (ocean precedes) to 3 year (ocean follows) illustrate well the nature of the dominant air-sea interactions (Fig. 6). When the oceanic variables precede PC1 by 1 year (or more), none of the correlations seems significant, but when they are in phase or follow by up to a few years, the correlations are large. As in Fig. 3, the correlations with p_{bc} (left) are strong at zero lags, peak when the ocean follows by 1 year, and slowly decrease with increasing lag. The spatial pattern at lag 0 and 1 mimic EOF1 of p_{bc} and represents nearly as much variance, confirming that the gyre variability is primarily wind-driven. The weakening of the Ekman pumping in the subtropical gyre and the Ekman suction in the subpolar gyre leads to weaker circulation of both gyres. Westward propagation is seen south of 35°N, consistently with that of a first baroclinic mode Rossby wave, but not at higher latitudes. At lag 0, the correlation of curl τ/f PC1 with surface current (middle left) clearly reveals Ekman current divergence. As the Ekman currents have the same short time scale as the wind stress, their influence vanish at positive lags and the correlation is then dominated by the more persistent geostrophic currents, with a spatial pattern consistent with the p_{bc} maps. The resulting modulation of the surface layer is likely to be responsible for the slight SST redness at low frequencies, although the correlation maps are too noisy to show obvious correspondences. The SST field (middle right) is also strongly correlated at zero lag with curl τ/f PC1, but the correlation decays more rapidly with increasing lag, as expected from the limited SST persistence. Note that the SST correlation pattern primarily mimics the patterns of the surface heat exchanges (right) and the Ekman currents that are associated with curl τ/f PC1, as expected from mixed-layer dynamics. The change of sign in the correlation with the surface heat flux between lag 0 and 1 (right column) shows that the latter contributes to the damping of the SST anomalies after they have been generated, as in the observations (Frankignoul et al. 1998).

3.3 Maximum covariance analysis

To increase the signal-to-noise ratio, we performed a maximum covariance analysis based on a singular value decomposition (hereafter SVD) in lead and lag conditions, using SST and several atmospheric variables (surface pressure, zonal wind stress, and temperature at 850 mb). A lagged SVD was also made between p_{bc} and surface pressure. Thus, an oceanic field $\boldsymbol{X}(t)$ at time t and an atmospheric one $\boldsymbol{Y}(t-\tau)$ at time $t-\tau$ are expanded into orthogonal signals

$$\boldsymbol{X}(t) = \sum_{1}^{K} a_k(t)\boldsymbol{p}_k, \quad \boldsymbol{Y}(t-\tau) = \sum_{1}^{K} b_k(t-\tau)\boldsymbol{q}_k \ ,$$

plus noise, with $\boldsymbol{p}_k \cdot \boldsymbol{p}_l = \delta_{kl}$, $\boldsymbol{q}_i \cdot \boldsymbol{q}_j = \delta_{ij}$, where the covariance between a_k and b_k is maximum for $k = 1, 2, \ldots$ (for a discussion of the unlagged case, see Bretherton et al. 1992). Homogeneous maps for the ocean (the projection of $\boldsymbol{X}(t)$ onto $a_k(t)$) and heterogeneous maps for the atmosphere (the projection of $\boldsymbol{Y}(t-\tau)$ onto the same time series $a_k(t)$) are shown since they preserve linear relations between the variables, which is not always the case between homogeneous or between heterogeneous maps (Newman and Sardeshmukh 1995). Homogeneous and heterogeneous maps are rather similar in the present analysis. We only considered the first two SVD modes. Robustness was assessed as in Venegas et al. (1996) by testing the statistical significance of the square covariance associated with each mode, using a Monte Carlo approach. Each SVD analysis was repeated 100 times, linking the original SST (p_{bc}) data set with randomly scrambled atmospheric data sets, so that the chronological order between the ocean and the atmosphere was destroyed. To prevent influencing the randomized square covariance by the oceanic persistence, a minimum separation of 20 (40) year was maintained between the SST (p_{bc}) field and the atmospheric ones. The quoted significance levels indicate the

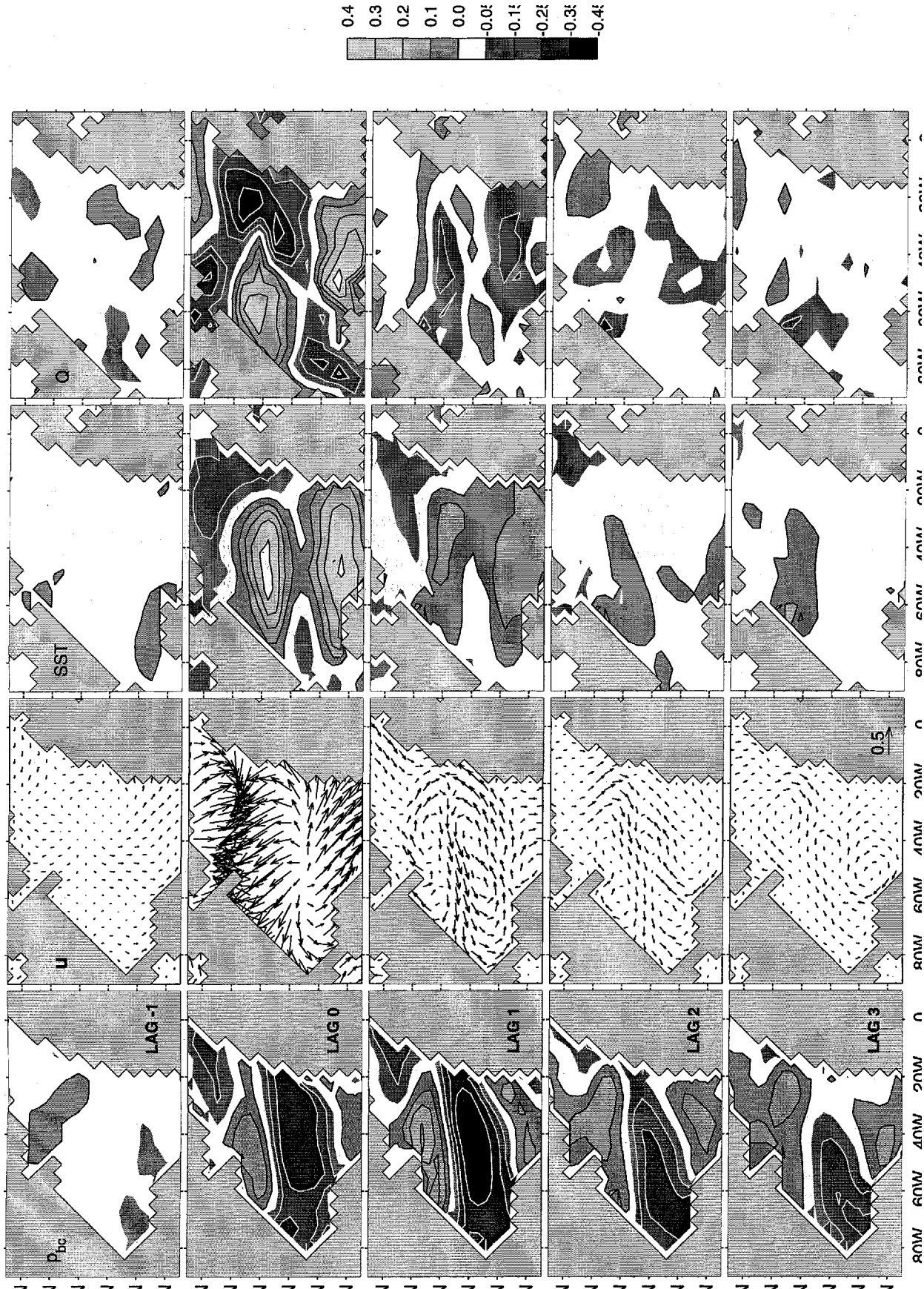

Fig. 6 Correlation map of curl τ/f PC1 with, from left to right, p_{bc}, horizontal surface current, SST, and net surface heat flux into the ocean at lags ranging between –1 year (ocean precedes) and 3 year (ocean follows). The correlation vectors for surface current are constructed from the correlation of its zonal and meridional components. Positive (negative) isolines are in *black* (*white*)

percentage of randomized square covariance for the corresponding mode that exceed the value being tested. Note that in the purely random case with no true covariance between ocean and atmosphere, the main SVD patterns should mostly resemble the dominant EOFs of each field, but without any preferred sign association between them. When the ocean leads the atmosphere (negative lags), the square covariance is usually small. Hence, in such low signal-to-noise situations, the stability and repeatability of a pair of patterns with consistent signs may be as good an indicator of a true covariance as the significance level of the square covariance. In the following, only significant and repeatable results in each half of the run are presented.

The strongest covariance between SST and the atmosphere is found at lag 0, and it slowly decreases with increasing lag when SST follows, as seen by the decreasing amplitude in the SVD patterns. The SVD between SST and surface pressure illustrates that the patterns are consistent with the atmospheric forcing of the ocean, since cold (warm) SST is found under northerly (southerly) wind. In the first SVD mode (Fig. 7), the SST pattern is like SST EOF2, but shifted slightly southward, and the surface pressure pattern largely corresponds to surface pressure EOF1. When SST lags surface pressure, the patterns remain similar but for a slow northeastward SST migration which seems largely consistent with the mean currents in Fig. 5. The square covariance remains highly significant until lag 5, and by then the SST pattern resembles that at lag zero, but with the opposite sign (and a stronger northward lobe). This approximate sign reversal causes an "advective resonance" of the kind investigated by Saravanan and McWilliams (1998) and may explain why a 10-year oscillation is found in the MSSA. Note that the SST persistence is larger than suggested by the correlation analysis, as the signal-to-noise ratio is smaller for grid point data, and by the auto-correlation of the PCs, as a single EOF cannot represent the SST propagation. In the second SVD mode (Fig. 8), the pattern of SST at lag 0 resembles SST EOF1, and that of surface pressure its EOF2. The SST persistence is somewhat smaller than in Fig. 7, and no propagation can be seen, perhaps because the surface current is small near 45°N where the SST signal is maximum.

Large-scale patterns of co-variability are also found in the dominant SVD modes when SST leads the atmosphere. In the first mode, the only significant covariability is found at lag −3 (Fig. 7), but similar patterns are seen at lag −4 and −2. The SST and surface pressure patterns at lag −3 resemble those at lag 0, but for a change of sign and a smaller amplitude, and similar results are found when using the other atmospheric variables in the SVD. This sign reversal between positive and negative lags is not indicative of a negative feedback, however, but rather of a damped standing oscillation. Indeed, as recalled already, in the former case the covariance when the ocean leads should peak at lag −1 and decay at larger negative lags, while in Fig. 7 the peak occurs at lag −3. Furthermore, the evolution of the lag −3 SST pattern was estimated (not shown) by projecting its normalized time series onto the SST field shifted forward by 1, 2, and 3 year. It showed that, instead of decaying as in a negative feedback case, the SST signal weakens after 1 year, disappears after 2 year, but (coarsely) reappears with the reversed sign at year 3. This suggests that the mode has an oscillatory component with a period of about 6 year. Since a negative auto-correlation is only seen at lag 3 for the atmospheric PCs (Fig. 3), and the 6-year period is most clearly singled out for surface pressure in the MSSA below, the quasi-oscillatory behavior is likely originate in the atmosphere. Whether or not it is sustained by air-sea interactions could not be established.

Fig. 7 Homogeneous map for SST (in K, *left*) and heterogeneous map for surface pressure (in Pa, *right*) for the first dominant SVD mode at lags between −3 and 5 years (positive when the ocean follows) when the significance level (*upper left side*) is below 20%. The SVD times series were normalized so that the maps indicate typical amplitudes. Positive (negative) isolines are in *black* (*white*). *Lag*, *mode number*, *correlation* and *significance* are indicated

As seen in Fig. 8, a non-random behavior of a different nature is found at lag −3 to −5 in the second SVD mode between SST and surface pressure. Indeed, the significant patterns (albeit with low confidence level) remain similar to, and of the same sign as, the lag 0 ones, except for a small eastward shift of the surface pressure. This signature is suggestive of a randomly forced system which is quasi-stationary in space and sustained by a weak positive feedback (Sect. 3.1). It is not of an oscillatory nature.

Like the correlation analysis, the SVD between p_{bc} and surface pressure indicates that the thermocline variability primarily reflects the stochastic forcing of the ocean by the atmosphere, with the strongest covariance when p_{bc} lags by 1 year (Figs. 9 and 10). The first (second) SVD mode mainly describes the strengthening and expansion of the subpolar (subtropical) gyre in response to the atmospheric forcing, and in both cases there is a striking correspondence in location and sign between the main atmospheric and oceanic centers of action. The covariance remains highly significant when the ocean lags the atmosphere by as much of a decade, stressing the large persistence of the thermocline motions.

Although the largest square covariances are found at lags ≥0, the square covariance is mostly larger than expected by chance when p_{bc} leads surface pressure by a few years, except at lag −1 which is affected by atmospheric persistence. In the first SVD mode (Fig. 9) which involves a surface pressure pattern similar to that in Fig. 7 (or surface pressure EOF1), there are highly significant covariances at lag −2 to −4, and as in Fig. 7 they show a change of sign with the lag 0 case, with only little change in pattern. However, at lag −4 the p_{bc} pattern differs and there is a shift in the order of the SVD modes. As noted before, this is consistent with a slight oscilla-

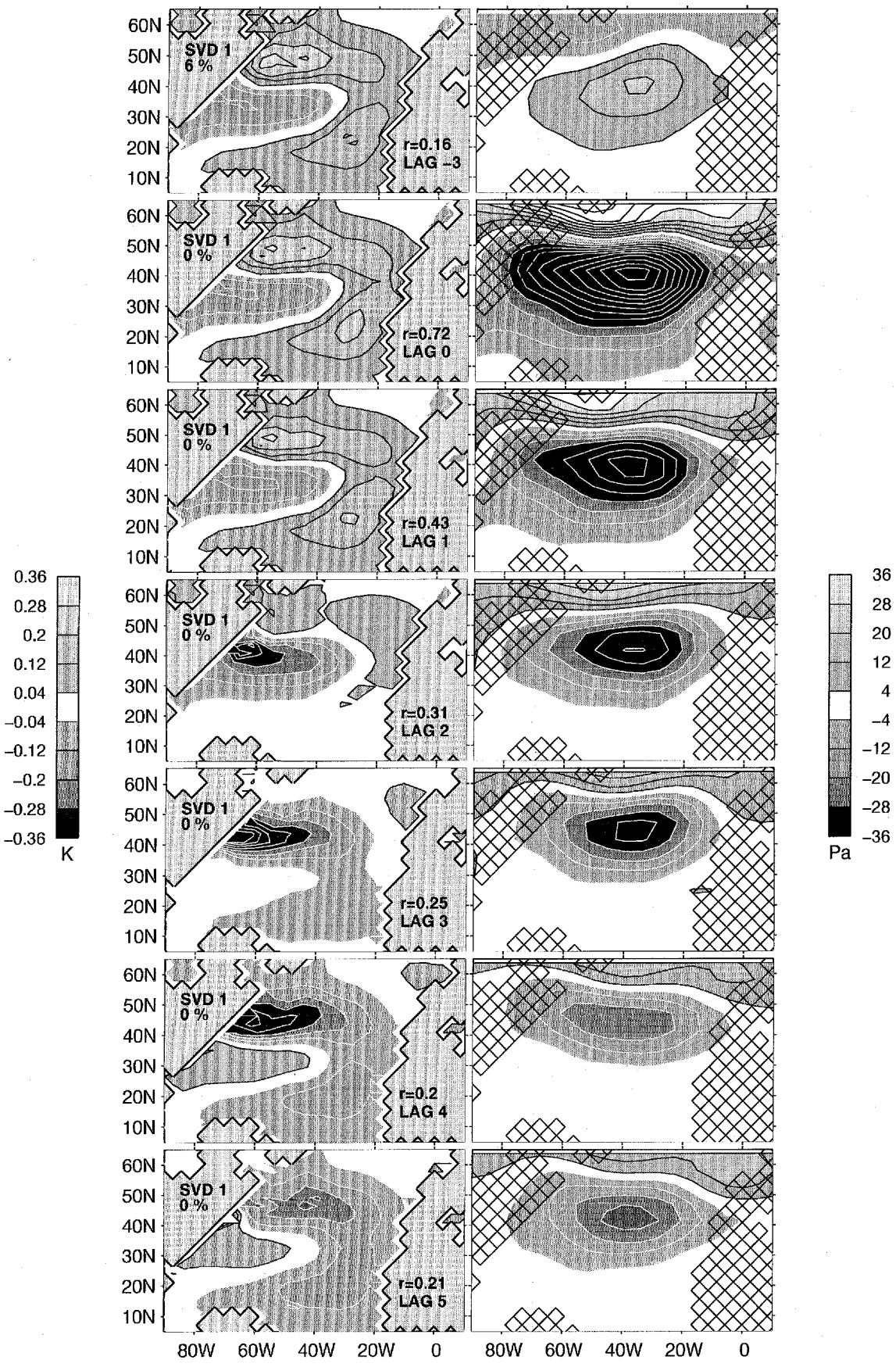
SVD 1
6 %
r=0.16
LAG –3
SVD 1
0 %
r=0.72
LAG 0
SVD 1
0 %
r=0.43
LAG 1
SVD 1
0 %
r=0.31
LAG 2
SVD 1
0 %
r=0.25
LAG 3
SVD 1
0 %
r=0.2
LAG 4
SVD 1
0 %
r=0.21
LAG 5
60N
50N
40N
30N
20N
10N
80W
60W
40W
20W
0
0.36
0.28
0.2
0.12
0.04
–0.04
–0.12
–0.2
–0.28
–0.36
K
36
28
20
12
4
–4
–12
–20
–28
–36
Pa

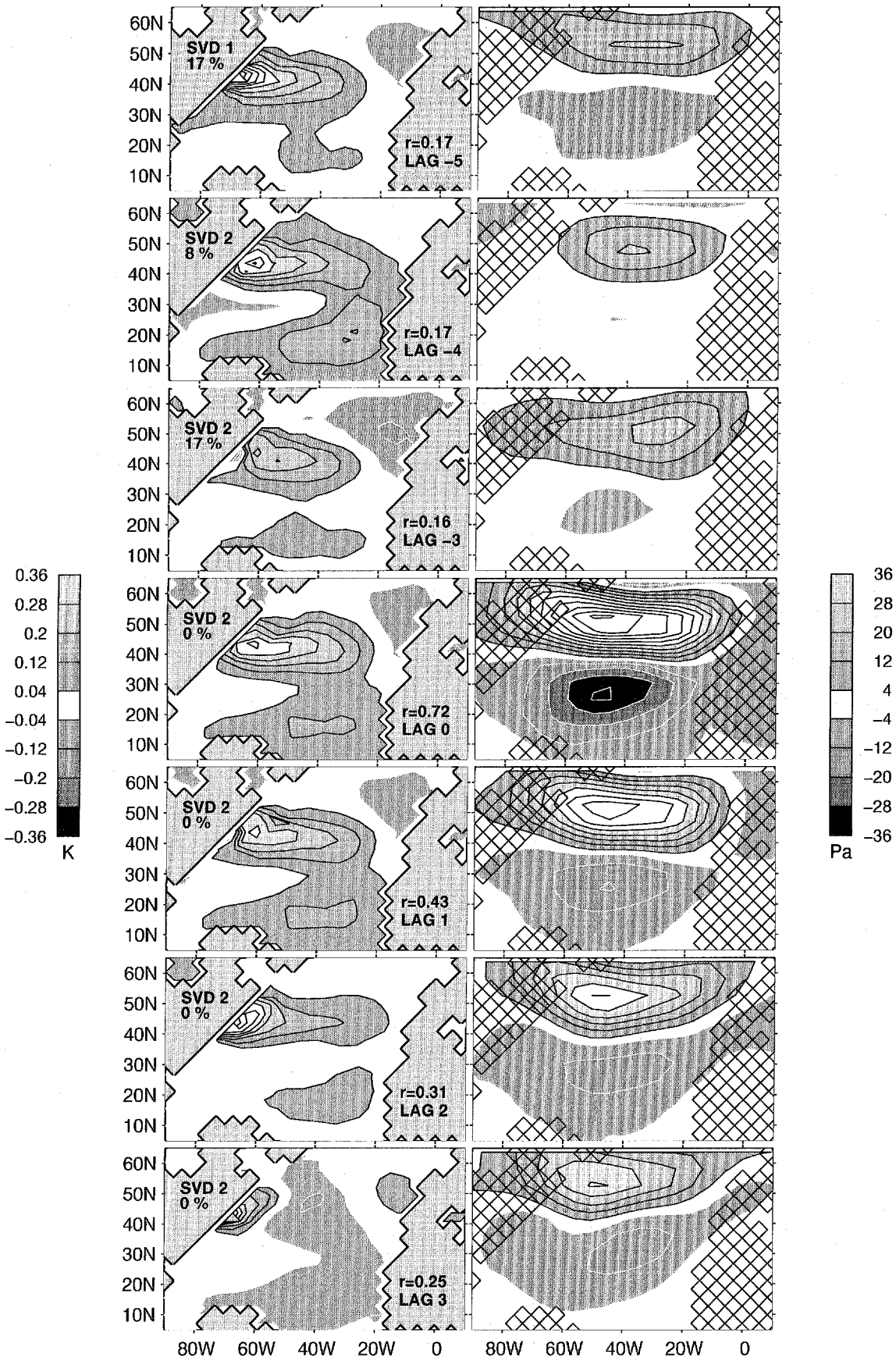
SVD 1
17 %
r=0.17
LAG –5
SVD 2
8 %
r=0.17
LAG –4
SVD 2
17 %
r=0.16
LAG –3
SVD 2
0 %
r=0.72
LAG 0
SVD 2
0 %
r=0.43
LAG 1
SVD 2
0 %
r=0.31
LAG 2
SVD 2
0 %
r=0.25
LAG 3
60N
50N
40N
30N
20N
10N
80W
60W
40W
20W
0
0.36
0.28
0.2
0.12
0.04
–0.04
–0.12
–0.2
–0.28
–0.36
K
36
28
20
12
4
–4
–12
–20
–28
–36
Pa

◀

Fig. 8 As in Fig. 7, but for the second dominant SVD mode at lags between −5 and 3 years

tory component in the decadal variability of the two media. In the second SVD mode (Fig. 10) which involves the surface pressure pattern of Fig. 8 (or EOF2), there are highly significant covariances at lag −3 and −4 (and less significant ones at lag −2 and −5). As in Fig. 8, they show no change of sign between lead and lag conditions and only little changes in the patterns, primarily an emphasis of the subpolar gyre at lag −4 and a slight eastward surface pressure shift. An atmospheric high (low) is thus associated with a similarly located oceanic high (low) a few years before, as expected from a positive feedback that would reinforce the fluctuations in the two media. The same behavior can thus be recognized in Figs. 7 and 9, and in Figs. 8 and 10, showing that the thermocline plays a key role in the decadal variability. That the evidence for positive feedback is stronger in the SVD with p_{bc} than in that with SST (compare the significance level) results presumably from the lesser amount of high frequency variability in the p_{bc} data.

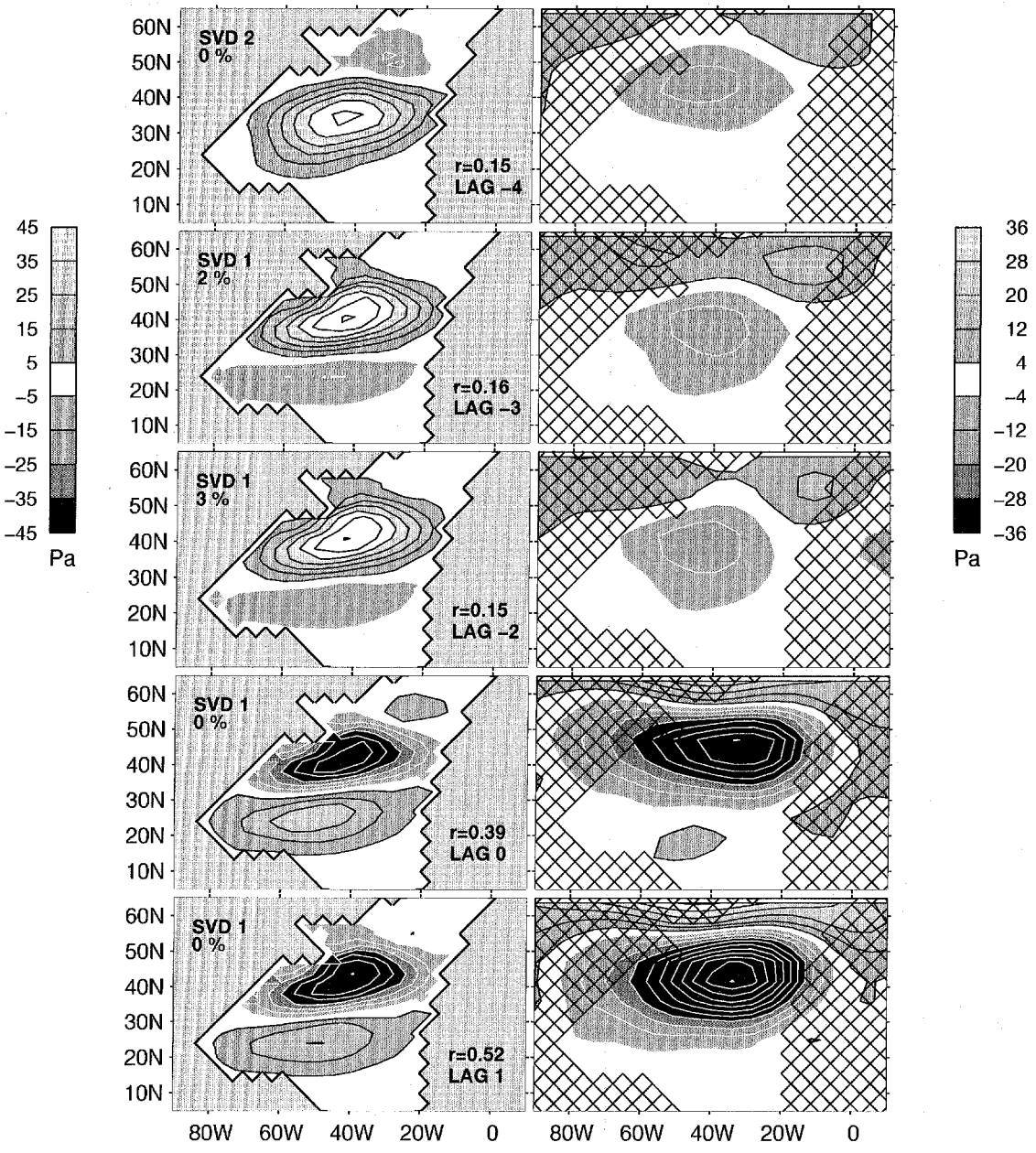

Fig. 9 Homogeneous map for p_{bc} (in Pa, *left*) and heterogeneous map for surface pressure (in Pa, *right*) for the dominant SVD mode at lags between −4 and 1 years (positive when the ocean follows) when their significance level (*upper left side*) is below 5%. The SVD times series were normalized so that the maps indicate typical amplitudes. Positive (negative) isolines are in *black* (*white*). *Lag*, *mode number*, *correlation* and *significance* are indicated

3.4 Multichannel singular spectrum analysis

To check if some of these features could be detected by other methods, we also used MSSA, which is designed to reveal intermittent oscillatory behaviors in multivariate time series. The core of the technique is a based on diagonalizing the lagged covariance matrix of the time series, which is equivalent to performing an EOF analysis of a series of extended vectors consisting of the original field taken at M successive times, M being the window length. The EOFs are then sequences of M maps (extended EOFs), and their time behavior is described by a PC which reflects the strong filtering inherent to the method (Vautard and Ghil 1989). Plaut and Vautard (1994) have shown that two almost equal eigenvalues of the lagged covariance matrix correspond to pairs of extended EOFs with their PC in quadrature, defining an oscillation in phase space whose evolution can be re-projected onto the physical space. MSSA was applied to the surface pressure and SST data, both jointly and separately, after filtering each field by a standard EOF analysis to reduce their dimension and retaining about 70% of the variance of each field (the stability of the results was verified with other truncation choices). The search for oscillatory modes used the phase quadrature property, only retaining couples of PCs with a lagged correlation exceeding 0.5 over at least two periods. To help distinguishing robust oscillations from the numerous and changing ones that are identified by the method, different window lengths (20, 28, 34, 40, 45, 50, and 55 years) were considered and the analysis repeated in each half of the run, even though the stability of oscillatory behaviors between independent realisations is not sufficient grounds to conclude that data exhibits oscillations (Allen and Robertson 1996).

None of the cases showed a strong oscillatory component. However, there was some evidence of weak but robust cyclical behaviors. The combined analysis of the two fields (equally weighted) mainly emphasized periods between 9 and 13 years. The patterns were very similar, but there was little repeatability between halves. Thus, the phenomenon seems broadband. As shown in Fig. 11, the patterns are nearly identical to those in Fig. 7, and there is also a hint of northeastward SST

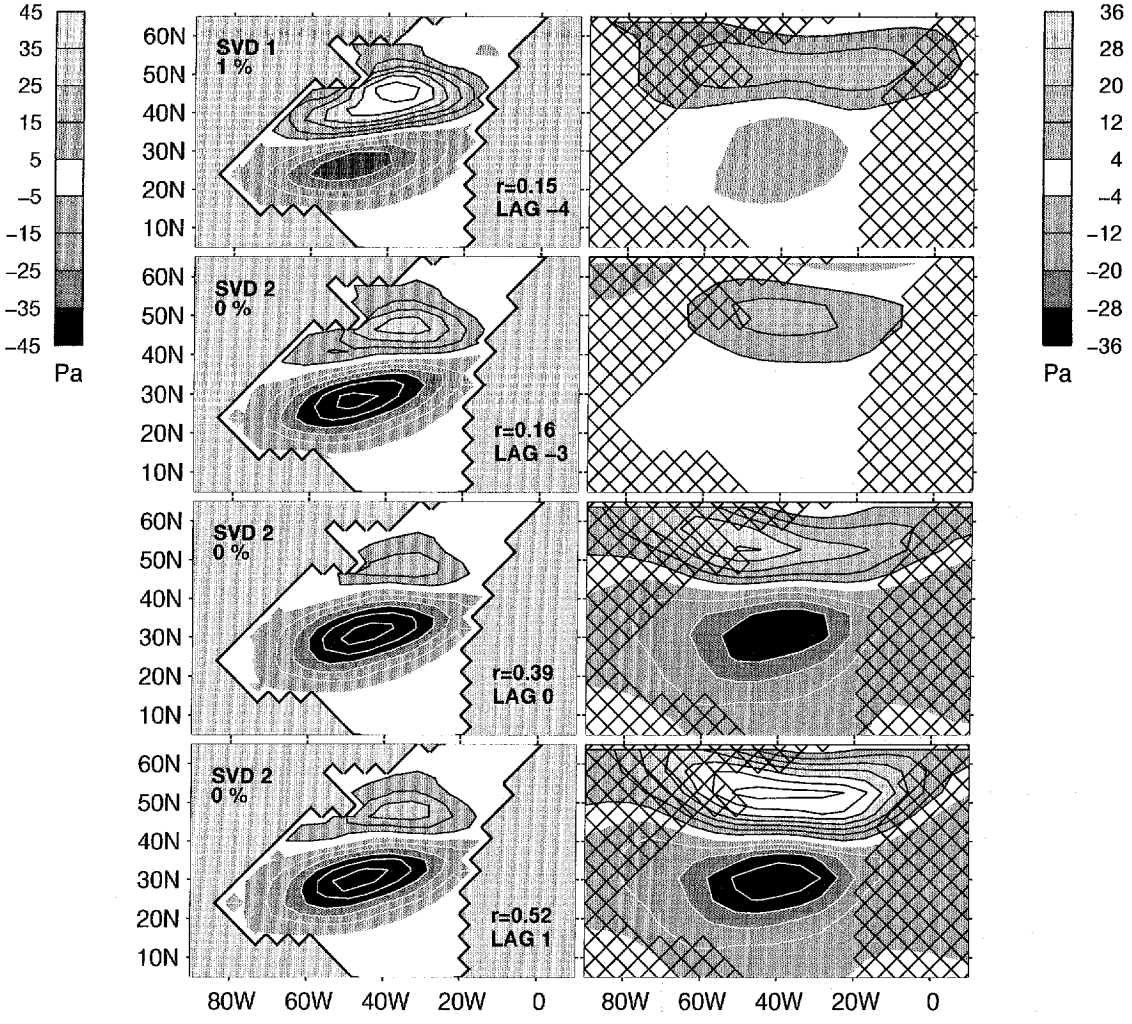

Fig. 10 As in Fig. 9 but for the second dominant mode

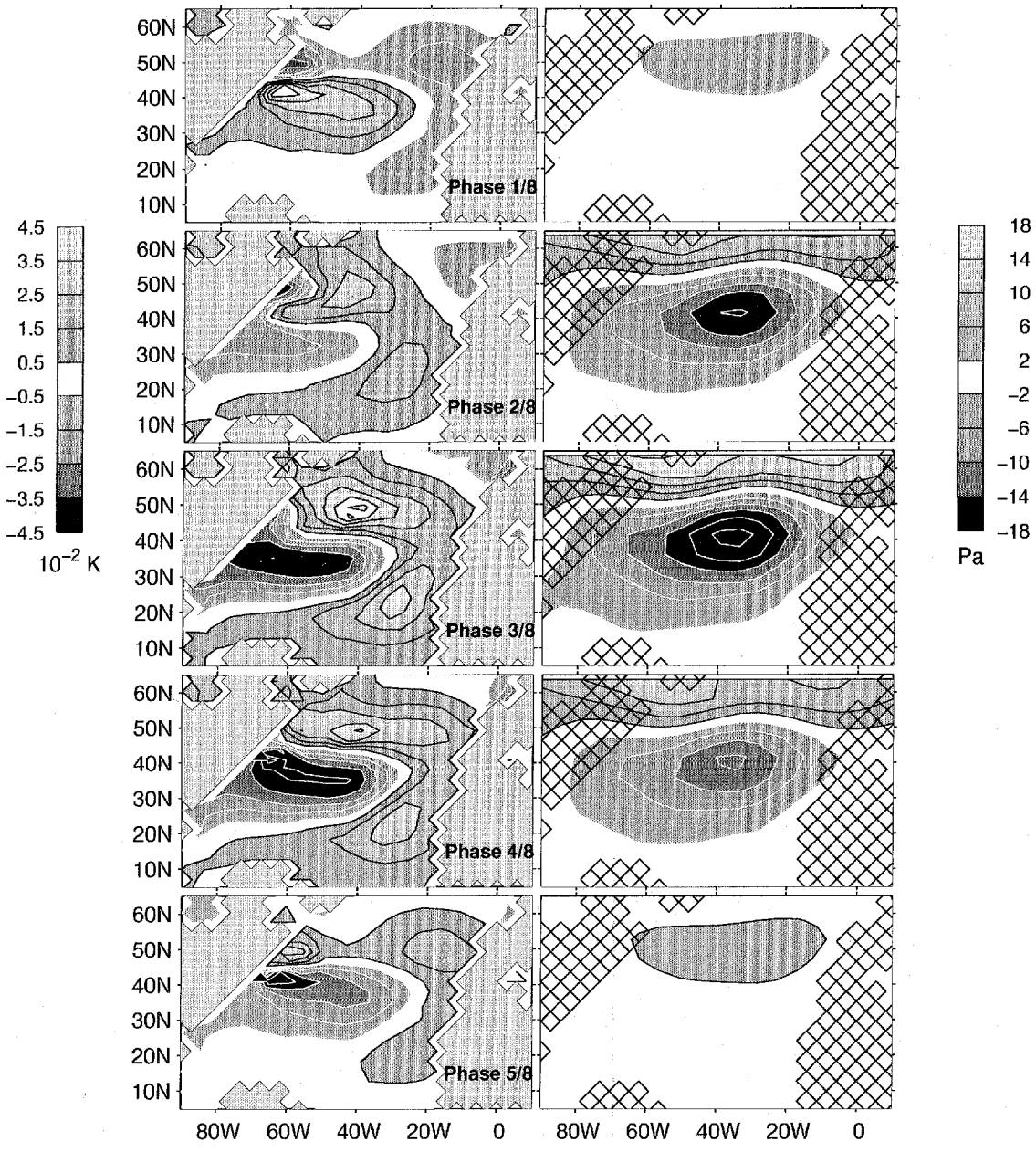

Fig. 11 Reconstructed patterns associated with the 9-year mode detected by a joined MSSA (pair 8–9, $M = 34$) of SST (*left*) and surface pressure (*right*) during a half cycle, so that the time interval between successive maps is slightly larger than a year (4 and 10 EOFs were retained for surface pressure and SST, respectively). The PCs are normalized so that the maps indicate typical amplitudes. Positive (negative) isolines are in *black* (*white*)

propagation, best seen between 30 and 40°N. A similar 10-year mode was detected by ZF in a combined analysis also including the baroclinic pressure, but that no trace of the (passive) 20-year mode of ZF could be found.

In the MSSA of surface pressure alone, an oscillatory component was identified for different M or truncations around periods of 6 and 9 years, with similar patterns to those in Fig. 11. The stronger 9-year variability was only seen in the first half of the record, however, but the 6-year period was robust and consistent with the weak atmospheric quasi-periodicity discussed. The MSSA of SST alone repeatedly suggested a weak oscillatory behavior at periods ranging between 9 to 12 year, again with similar patterns to those in Fig. 11. For a few choices of window length, a standing SST oscillation resembling the middle phase of Fig. 11 could also be recognized near 6-year period, presumably reflecting the SST response to the 6-year atmospheric oscillation, but it was not robust.

In summary, the MSSA is generally consistent with the lagged SVD. However, MSSA does not directly distinguish between cause and effect, while the lagged

SVD made it obvious that the main air-sea interaction was the atmospheric forcing of the ocean. On the other hand, MSSA showed that the weak 6-year periodicity discussed was primarily found in the atmosphere, while that around 10 years was mostly found in the SST, as expected from advective resonance. These MSSA modes have little energy, however, representing only a few % of the total variance. Note that MSSA showed no evidence of the positive ocean-atmosphere feedback suggested by Figs. 8 and 10, but this was expected since such interaction does not lead to cyclical behaviors.

4 The North Pacific variability

The air-sea interactions in the North Pacific were found to be very similar to those in the North Atlantic, except for a somewhat larger persistence of the main oceanic patterns. Fewer details will thus be given. Figure 12 documents the main patterns of variability of surface pressure (top), SST (middle), and p_{bc} (bottom), which are rather similar to those in the Atlantic, except for a larger scale. Although the yearly surface pressure PCs are slightly auto-correlated at lag 1 (above the 5% level), the atmospheric persistence being particularly strong in the southeastern part of the North Pacific, the atmospheric frequency spectra are again primarily white (Fig. 13). Marginally significant, but repeatable, peaks are seen at a period of 8 year for the two surface pressure EOFs and 14 year for EOF2 (the 20-year peak in EOF1 is only found during the second half). These tiny peaks are also present in the Ekman pumping.

For SST, a redder frequency spectrum than in the Atlantic is found for the main PCs, presumably because of a stronger SST modulation by geostrophic motions (see later). Again, the oceanic PCs are cross-correlated at non-zero lags, suggesting propagation. There are also small spectral peaks which seem significant around 10, 8, and 5 year for PC1, but there is no trace of the 18-year peak found by Robertson (1996). The first PC of p_{bc} has a red spectrum with no significant peak (other than possibly a small one at 8-year period). Its dominant time scale is longer than the corresponding one in the Atlantic, as predicted from the larger basin size by linear theory (see FMZ). PC1 has limited lag-correlation with the other p_{bc} PCs, suggesting that the p_{bc} dipole in Fig. 12 is primarily standing. On the other hand, the second EOF describes a westward propagating monopole (2 to 3 cm/s at 35°N) which evolves into a tripole, as seen in Fig. 18 later.

Except for the larger persistence, the cross-correlation between atmospheric and oceanic PCs (or between atmospheric PCs and oceanic grid point data) is basically the same as in the North Atlantic. It primarily reflects the stochastic forcing of the ocean by the atmosphere, with the mixed layer responding rapidly and the thermocline more slowly. It indicates that the heat flux feedback is also negative in the North Pacific. The year-to-year SST changes are more strongly influenced by the current variability than in the North Atlantic, however, resulting in a stronger SST modulation by the gyre fluctuations. This is illustrated in Fig. 14 by the cross-correlation between the PC1s of SST and p_{bc}. Two different kinds of behavior can be recognized: a peak is seen when SST leads p_{bc} by 1 year because the SST responds faster to the atmospheric forcing than the thermocline (as in Fig. 3) and a large persistent correlation is found when p_{bc} leads SST because the low frequency geostrophic currents modulate the SST (see Robertson 1996). This strong modulation explains the large persistence of SST PC1.

The primarily passive role of the North Pacific ocean is well illustrated by the dominant mode of the lagged SVD between SST and surface pressure (Fig. 15). As in the North Atlantic, the square covariance is most significant when the two variables are in phase, and it slowly decays when SST lags. The surface pressure pattern at lag 0 is like its EOF1 while the SST pattern resembles SST EOF1, although the lobe around 35°N, 165°W is more pronounced. The mode is very persistent when SST lags, remaining significant down to lag 18, with the same surface pressure pattern but a slowly evolving SST one that reflects geostrophic modulation, not mean surface advection.

Prior SST influence on surface pressure was only found in the first SVD mode at lag −3, with limited significance but repeatability in two halves. This mode involves the same atmospheric pattern as at lag 0, but a more complex SST pattern change than in Fig. 7, although there is also an approximate sign reversal for the main SST lobe. However, the forward evolution of the lag −3 SST pattern (not shown) does not suggest an oscillation. Prior SST influence of a different nature is suggested by the SVD between SST and temperature at 850 mb (hereafter T_{850}), where the SST appears to be involved in a persistent two-way coupling. This is shown in Fig. 16 where the square covariance remains significant when SST lead T_{850} by as much as 9 years (the coupled mode appears as second SVD mode at lag −3 because the first one represents the approximate sign reversal discussed already). Note that the SST pattern at lag 0 and 1 is very similar to that in Fig. 15. Correspondingly, the same atmospheric mode than in Fig. 15 is involved since the surface pressure and T_{850} time series are highly correlated. The interaction is characterized by a close similarity in shape and sign between the SST and T_{850} patterns in lead and lag conditions, as expected from a positive feedback. The interaction may be slightly different from that detected in the North Atlantic since it is seen here in the SVD with T_{850} and not surface pressure, while it was the opposite in the North Atlantic. However, the positive feedback appears similarly in both oceans in the SVD between surface pressure and p_{bc}, as seen below. Presumably, it did not appear in Fig. 15 because the signal-to-noise ratio was too small.

The lagged SVD between p_{bc} and surface pressure shows that the thermocline primarily responds to the atmospheric forcing. The dominant thermocline mode is

a very persistent dipole whose pattern does not change until lag 11, except for a very slow westward displacement of the southern lobe (Fig. 17). As in the North Atlantic, there is a good correspondence in sign and location between the main center of action of the oceanic and the atmospheric pressure. The second SVD mode describes the thermocline response to an EOF2-like surface pressure pattern (Fig. 18). Although the response persists until lag 10, there are strong changes in the p_{bc} pattern which starts as a westward propagating monopole but evolves into a tripole since poles of opposite sign rapidly develop to the north and south, the latter also propagating westward.

Evidence of active air-sea coupling is found in the first SVD mode, where the square covariance remains significant between lag −7 and −19 (Fig. 17). The patterns are as at positive lags, except for a small northwestward shift in surface pressure, so that the atmospheric feedback sustains the dominant fluctuations it had generated, as in Fig. 16. As in the North Atlantic,

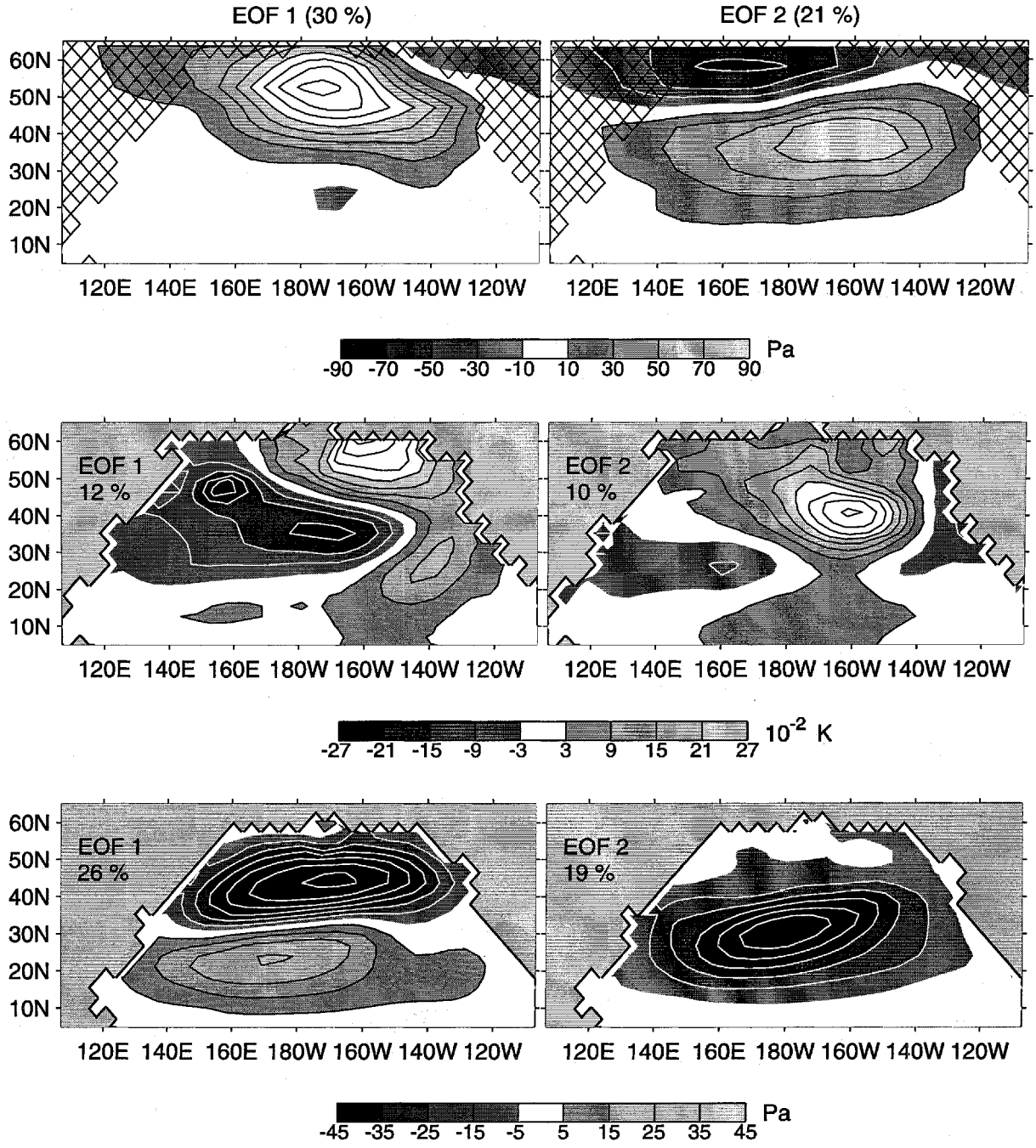

Fig. 12 First two EOFs of the yearly surface pressure (in Pa, *top*), SST (in 10^{-2} K, *middle*) and p_{bc} (in Pa, *bottom*) in the North Pacific region. The EOFs indicate typical amplitudes as the PCs are normalized. The EOF number and fractional variance are shown in each panel. Positive (negative) isolines are in *black* (*white*)

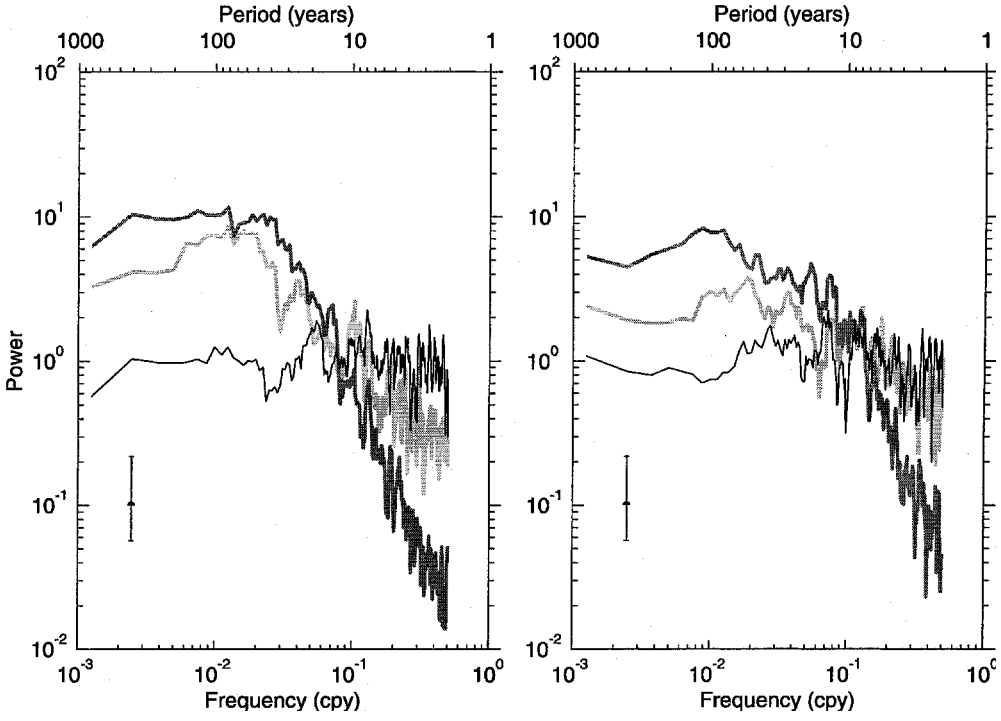

Fig. 13 Multitaper spectrum of the first (*left*) and second (*right*) PCs of surface pressure (*thin line*), SST (*gray*), and p_{bc} (*thick*) in the North Pacific. The error bars give the 95% confidence interval

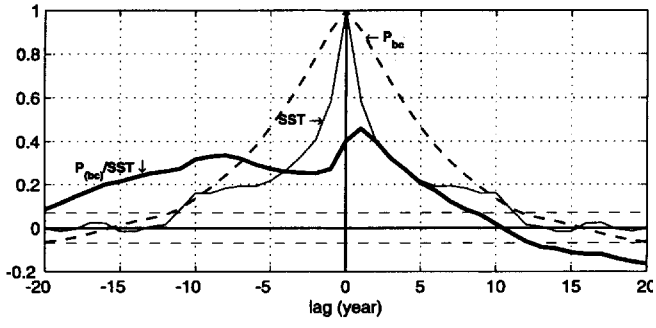

Fig. 14 Auto- and cross-correlation of the PC1s of SST and p_{bc}. The *dashed line* indicates the 5% level for zero correlation

the signature of the positive feedback is stronger in the thermocline than at the surface. Although the surface pressure pattern involved in the two-way coupling is a monopole in the North Atlantic (Fig. 10) and a dipole in the North Pacific (Fig. 17), the general structure of the coupled modes is similar and involves a simultaneous strengthening or weakening of the subtropical and subpolar gyres. Both modes also involve extratropical pressure perturbations of like-sign in the atmosphere and the ocean.

Robertson (1996) found in a MSSA of the first 500 years of the run that there were irregular ocean-atmosphere oscillations with a period of about 18 years. Except for a weak standing surface pressure mode at 8 years resembling surface pressure EOF1, we found no significant oscillatory behavior in the MSSA of surface pressure, SST, or the two variables together. For some window lengths, there was a suggestion of cyclical behavior in the combined field with a period of about 20 years (with patterns resembling those in Fig. 15), but the mode was neither robust nor repeatable in the two halves. Thus, the prominence of an 18-year mode in Robertson's (1996) analysis is artificial and due to the strong band-pass filtering (5–25 years) that he applied prior to MSSA. Indeed, a strong mode (pair 1–2) with a period of about 20 years was found in the MSSA of the present data set (combining SST, surface pressure, T_{850}, and p_{bc} to be in comparable conditions) when the same band-pass filter was applied.

Note that we have considered the North Pacific sector separately, although von Storch (1994) showed that the main mode of decadal variability in the North Pacific had a significant amplitude in the equatorial and south Pacific. However, although the main surface pressure and SST EOFs in Fig. 12 extend indeed throughout the whole basin, they have their largest amplitude in the Northern Hemisphere. We verified with a lagged SVD for the whole Pacific that it is primarily in the North Pacific that the ocean plays an active role. The same prior oceanic influence as in Figs. 15 and 16 was found when including the Pacific down to 40°S, but the amplitudes were much larger in the Northern Hemisphere.

5 Discussion

Our analysis of the low-frequency variability of the North Atlantic and the North Pacific in the full ECHAM1/LSG run confirms the ZF finding that the main air-sea interaction in the model is a passive response of the ocean to stochastic atmospheric forcing. The vari-

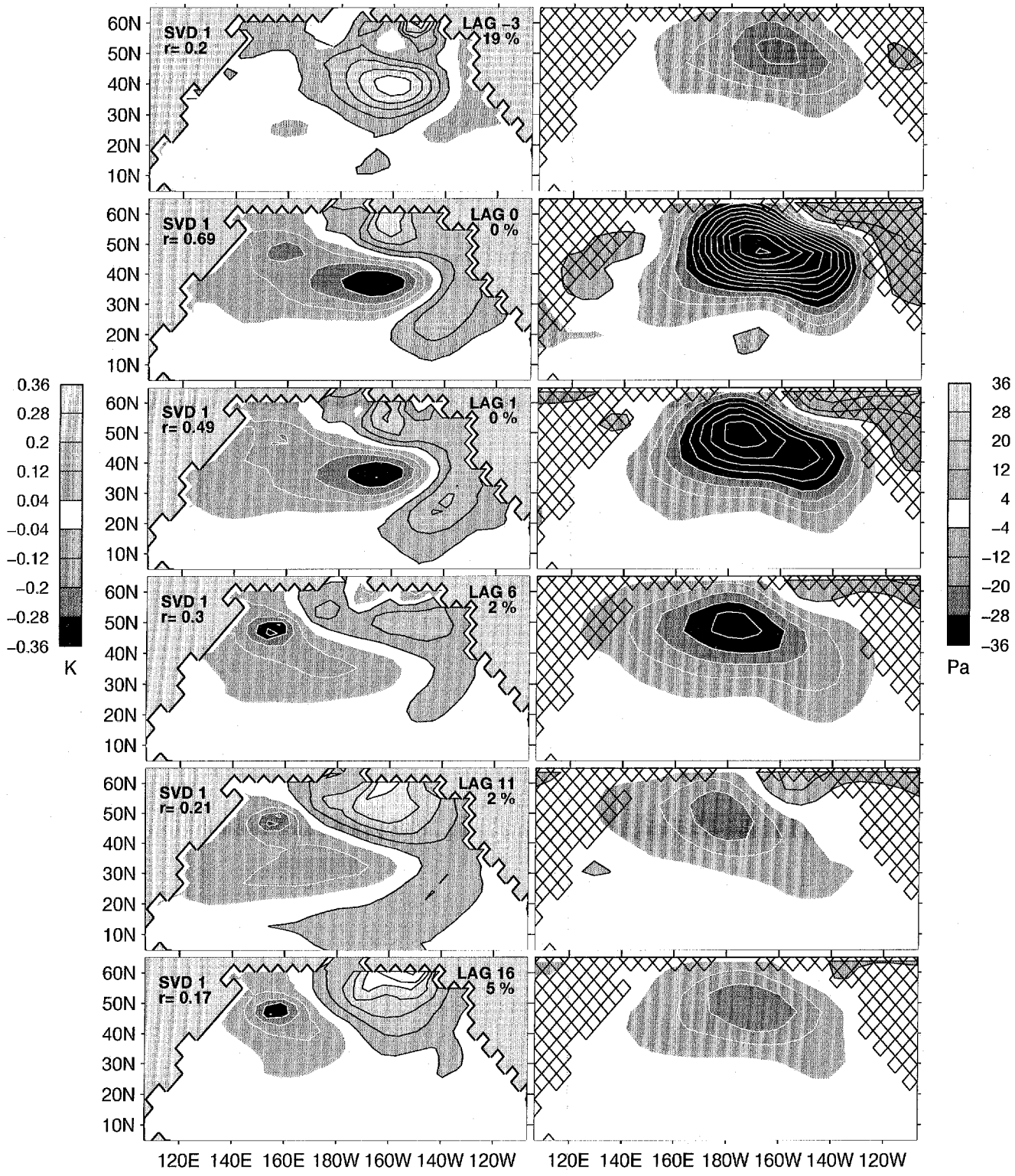

Fig. 15 Homogeneous map for SST (*left*) and heterogeneous map for surface pressure (*right*) for the first SVD mode at lags between −3 and 16 years (positive when the ocean follows) when the significance level (*upper left side*) is below 20% (shown every 5 years at positive lag). The SST time series were normalized so that the maps indicate typical amplitudes. Positive (negative) isolines are in *black* (*white*). *Lag*, *mode number*, *correlation* and *significance* are indicated

ability of the yearly averaged data is spread over a continuum of time scales, with a white frequency spectrum in the atmosphere but a red spectrum in the thermocline. Because of the SST modulation by the geostrophic fluctuations, which is particularly strong in the North Pacific, the SST spectra are slightly red, so

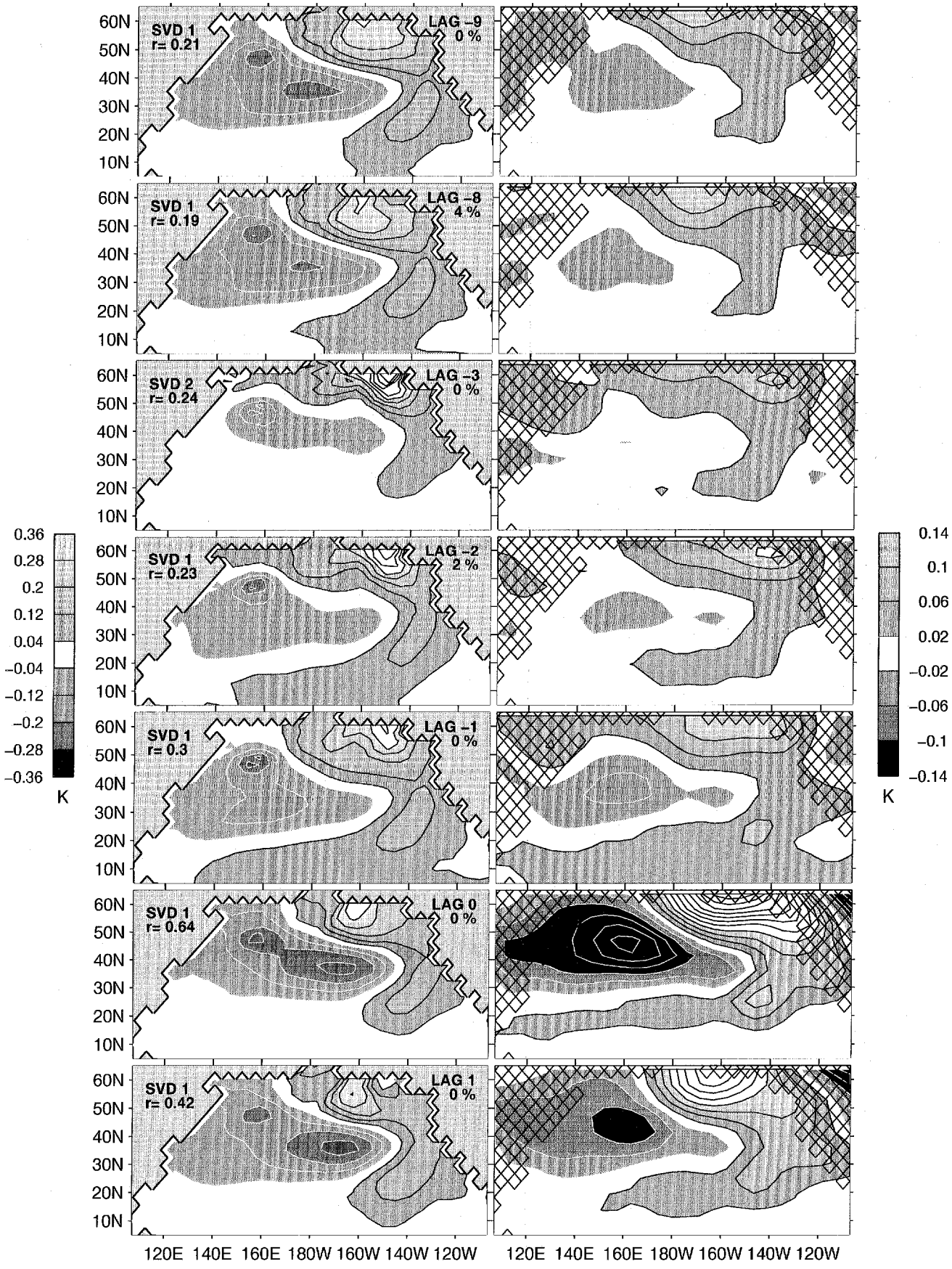

Fig. 16 As in Fig. 15 but for SST (*left*) and T_{850} (*right*) at lags ranging between −10 and 1 year

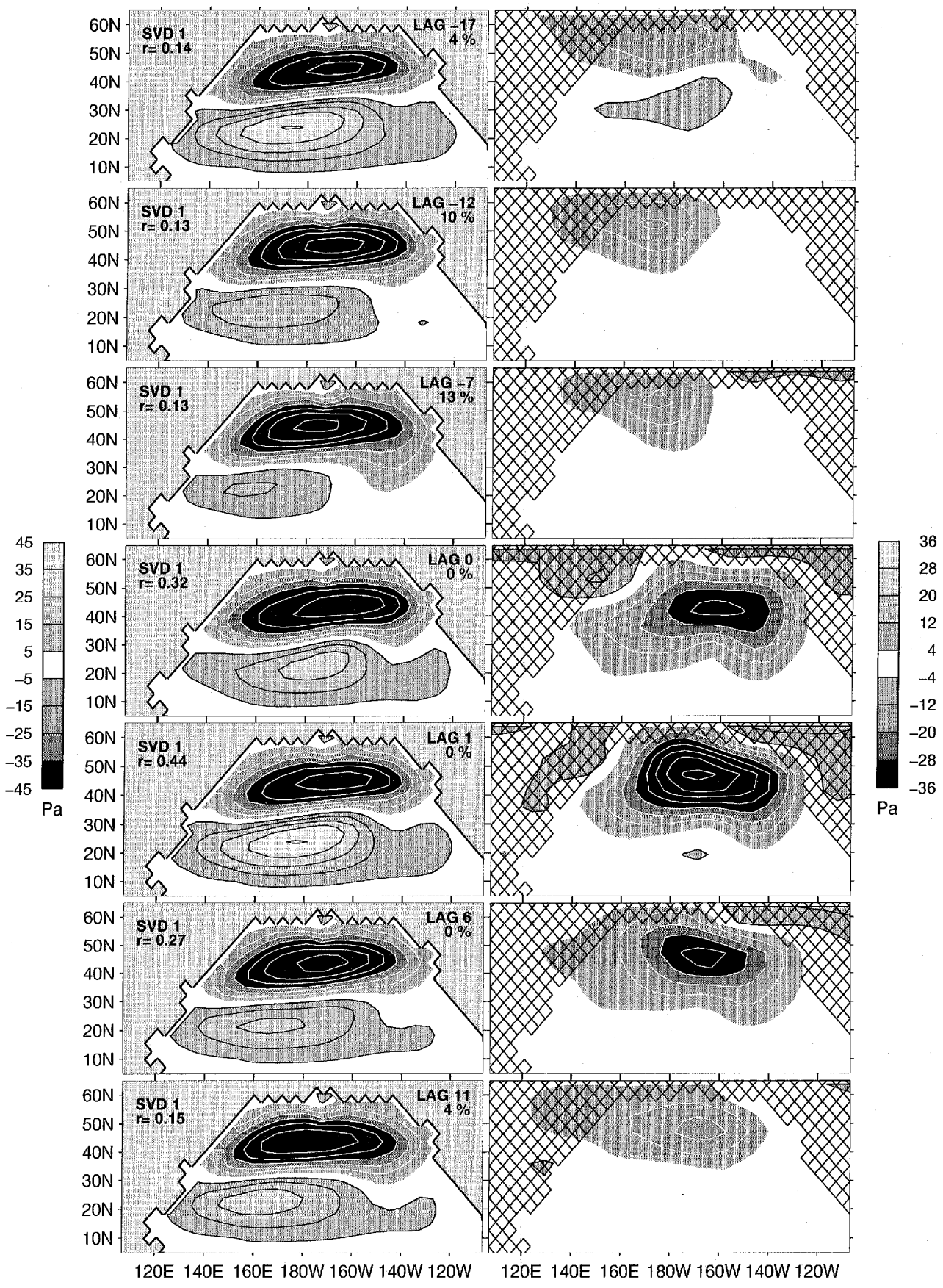
SVD 1
r= 0.14
LAG –17
4 %
SVD 1
r= 0.13
LAG –12
10 %
SVD 1
r= 0.13
LAG –7
13 %
SVD 1
r= 0.32
LAG 0
0 %
SVD 1
r= 0.44
LAG 1
0 %
SVD 1
r= 0.27
LAG 6
0 %
SVD 1
r= 0.15
LAG 11
4 %
60N
50N
40N
30N
20N
10N
120E 140E 160E 180W 160W 140W 120W
45 35 25 15 5 –5 –15 –25 –35 –45
Pa
36 28 20 12 4 –4 –12 –20 –28 –36
Pa

◀

Fig. 17 Homogeneous map for p_{bc} (*left*) and heterogeneous map for surface pressure (*right*) for the first SVD mode at lags ranging between −17 and 11 years (positive when the ocean follows) when the significance level (*upper left side*) is below 20%. The maps are shown every 5 years between lag −17 and −7, and 1 and 11. The time series were normalized so that the maps indicate typical amplitudes. Positive (negative) isolines are in *black* (*white*). *Lag*, *mode number*, *correlation* and *significance* are indicated

that it is the geostrophic variability that sets the decadal time scale. As predicted by FMZ, the dominant time scale is larger in the Pacific, but otherwise the air-sea interactions are similar in the two ocean sectors. Because the heat, momentum, and vorticity fluxes at the sea surface are correlated in space and time, the SST variability is directly linked to that in the ocean interior. As the SST responds more rapidly to the atmospheric forcing, yearly data tends to be in-phase with atmosphere while the thermocline fluctuations lag by 1 year. However, the SST modulation by the latter results in persistent correlation between the two fields when SST follows.

The ocean is not only passive in the ECHAM1/LSG model, however, as a clear indication of an active, albeit very weak, coupling between the ocean and the atmosphere was found in both oceans. A weak positive feed-

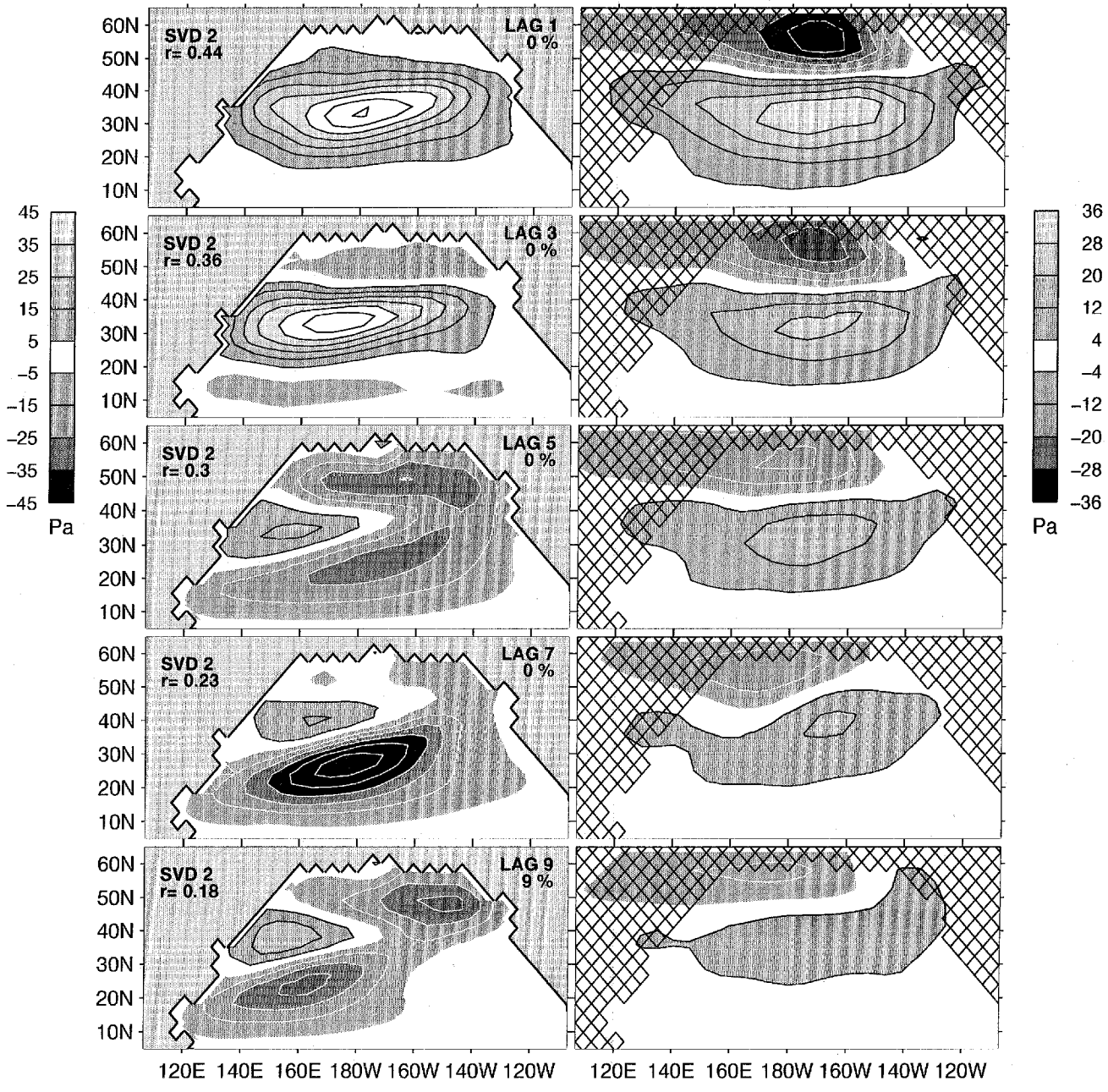

Fig. 18 As in Fig. 17 for the second mode

back contributes to enhancement of the second dominant surface pressure mode (with a NAO-like pattern) in the North Atlantic and the first one in the North Pacific. In both cases, the interaction involves the geostrophic variability via its response to Ekman pumping and its modulation of the SST. Although the surface pressure pattern is a monopole in the North Atlantic and a dipole in the North Pacific, the oceanic changes similarly involve the strengthening (or weakening) of the subtropical and subpolar gyres, and in both cases there is a good correspondence in sign and location between the main centers of action of the oceanic and the atmospheric pressure. This suggests that the dynamics are similar in the two ocean sectors. These interactions are too weak to redden the atmospheric spectra, however, and they could only be detected by using such a powerful technique as lagged SVD.

Although weaker, the two-way coupling bears some similarity with that found in the higher resolution HOPE model (Latif and Barnett 1994). However, here the surface heat flux feedback is negative, while a positive heat flux feedback is an important (if questionable) part of Latif and Barnett's (1994) scenario. In ECHAM1/LSG, the positive feedback between the ocean and the atmosphere occurs via the wind stress, overcoming the negative heat flux feedback. It involves the Ekman pumping, the response of the gyres, and their modulation of the SST. Presumably, the diabatic heating which results from the SST damping by the surface heat exchanges is strong enough to generate an atmospheric response which reinforces the Ekman pumping. Whether the wind stress feedback occurs as in the simple linear model of Goodman and Marshall (1999) or in a more complex fashion requires more fundamental studies.

In the North Atlantic sector, a weak 6-year periodicity was identified in the dominant mode of variability, both by conventional methods and by MSSA, and it is likely to originate in the atmosphere. In addition, advective resonance creates some oscillatory behavior in the SST near the 10-year period. However, the associated variance is very small. Similarly, a few small peaks were found in the North Pacific, but there was no indication of the robust 18-year oscillatory behavior claimed by Robertson (1996), which was due to band-pass filtering. Note that decadal periods that are comparable to those discussed here have been identified in the observations (mostly in the Atlantic, see e.g., Mann and Park 1996; Moron et al. 1998), but the latter oscillations are also weak and changeable.

Here we have considered the North Atlantic and the North Pacific sectors separately. However, we have verified that the correlation between the two sectors is limited. For instance, the only significant correlation between the surface pressure EOFs in Fig. 1 and Fig. 12 is between North Atlantic EOF1 and North Pacific EOF2 ($r = 0.3$), besides a small ($r = 0.1$) correlation between the EOF1s. To a coarse approximation, the two basins can thus be analyzed separately, although there are small inter-basin teleconnections. Similarly, one can focus on the Northern Hemisphere. This is due in part to the weak variability of the ECHAM1/LSG model in the equatorial regions, which is a major shortcomings of the model. However, the lack of a significant ENSO cycle in the model has allowed us to easily analyze North Pacific modes which may otherwise be difficult to investigate.

In summary, although the ocean is primarily passive in ECHAM1/LSG, we have found interesting midlatitude coupled dynamics at the decadal scale. However, the departures from a passive behavior are weak and variable, and the potential predictability negligible. This may not be true in the real world, nor in other coupled models. If the extratropical ocean is passive in the GFDL model (Delworth 1996), it is active in ECHAM3/HOPE (Latif and Barnett 1994) and ECHAM3/LSG (Timmermann et al. 1998). Since the atmospheric component of the GFDL model responds little to midlatitude SST anomalies (Kushnir and Held 1996), while ECHAM3 responds very strongly (e.g., Latif and Barnett 1994), the sensitivity of the atmospheric components to SST changes may largely determine the strength of the decadal coupling. Thus, an assessments of decadal predictability must rely on more realistic models. Nonetheless, we hope that the present study will contribute to developing the methodological approaches that are needed to understand the complex behavior of the climate system.

Acknowledgements The GCM integration was made at the Max-Planck-Institut für Meteorologie in Hamburg and provided by J. von Storch, whose help is gratefully acknowledged. Thanks are due to F. Bonjean, A. Czaja, E. Maier-Reimer, U. Mikolajewicz, R. Vautard, E. Zorita, and many MILLENNIA participants for useful discussions. This research was supported by EEC grants ENV4-CT95-0101 and ENV4-CT98-0714.

References

Allen MR, Robertson AW (1996) Distinguishing modulated oscillations from coloured noise in multivariate datasets. Clim Dyn 12: 775–784

Allen MR, Smith LA (1996) Monte Carlo SSA: detecting irregular oscillations in the presence of colored noise. J Clim 9: 3373–3404

Bretherton CS, Smith C, Wallace JM (1992) An intercomparison of methods for finding coupled patterns in climate data. J Clim 5: 541–560

Cubasch U, Hasselmann K, Hoeck H, Maier-Reimer E, Mikolajewicz U (1992) Time dependent greenhouse warming computation with a coupled ocean-atmosphere model. Clim Dyn 8: 55–69

Delworth TL (1996) North Atlantic variability in a coupled ocean-atmosphere model. J Clim 9: 2356–2375

Frankignoul C, Hasselmann K (1977) Stochastic climate models. II. Application to sea-surface temperature variability and thermocline variability. Tellus 29: 284–305

Frankignoul C, Müller P, Zorita E (1997) A simple model of the decadal response of the ocean to stochastic wind forcing. J Phys Oceanogr 27: 1533–1546

Frankignoul C, Czaja A, L'Heveder B (1998) Air-sea feedback in the North Atlantic and surface boundary conditions for ocean models. J Clim 11: 2310–2324

Gates WL, Cubasch U, Meehl GA, Mitchell JB, Stouffer R (1993) An intercomparison of selected features of the control climates simulated by coupled ocean-atmosphere general circulation

models. Report of the Steering Group on Global Climate Modelling, WMO, 51 pp
Goodman J, Marshall J (1999) A model of decadal middle-latitude atmosphere-ocean coupled modes. J Clim 12: 621–641
Grötzner A, Latif M, Barnett TP (1998) A decadal climate cycle in the North Atlantic ocean as simulated by the ECHO coupled GCM. J Clim 11: 831–847
Kushnir Y, Held IM (1996) Equilibrium atmospheric response to North Atlantic SST anomalies. J Clim 9: 1208–1220
Latif M, Barnett TP (1994) Causes of decadal climate variability in the North Pacific/North American sector. Science 266: 634–637
Maier-Reimer E, Mikolajewicz U, Hasselmann K (1993) Mean circulation of the Hamburg LSG OGCM and its sensitivity to the thermohaline surface forcing. J Phys Oceanogr 23: 731–757
Mann ME, Park J (1996) Joint spatiotemporal modes of surface temperature and sea level pressure variability in the Northern Hemisphere during the last century. J Clim 9: 2137–2162
Moron V, Vautard R, Ghil M (1998) Trends, interdecadal and interannual oscillations in global sea-surface temperatures. Clim Dyn 14: 545–569
Newman M, Sardeshmukh PD (1995) A caveat concerning singular value decomposition. J Clim 8: 352–360
Percival DB, Walden AT (1993) Spectral analysis for physical applications. Cambridge University Press, Cambridge, UK, 583 pp
Plaut G, Vautard R (1994) Spells of low-frequency oscillations and weather regimesin the Northern Hemisphere. J Atmos Sci 51: 210–236
Robertson AW (1996) Interdecadal variability over the North Pacific in a multi-century climate simulation. Clim Dyn 12: 227–241
Roeckner E, Arpe K, Bengtsson L, Brinkop S, Dümenil L, Esch M, Kirk E, Lunkheit F, Ponater M, Rockel B, Sausen R, Schlese U, Schubert S, Windelband M (1992) Simulation with the present day climate with the ECHAM model: impact of model physics and resolution. Max-Planck-Institut für Meteorologie Rep 93, Hamburg, Germany, 171 pp
Saravanan R, McWilliams JC (1998) Advective ocean-atmosphere interactions: an analytical stochastic model with implications for decadal variability. J Clim 11: 165–188
Timmermann A, Latif M, Voss R, Grötzner A (1998) Northern hemispheric interdecadal climate variability: a coupled air-sea mode. J Clim 11: 1906–1931
Vautard R, Ghil M (1989) Singular spectrum analysis in nonlinear dynamics with applications to paleoclimatic time series. Physica D 35: 395–424
Venegas SA, Mysak LA, Straub DN (1996) Evidence for interannual and interdecadal variability in the South Atlantic. J Geophys Res 23: 2673–2676
Von Storch J (1994) Interdecadal variability in a global coupled model. Tellus 46A: 419–432
Von Storch JS, Kharin VV, Cubasch U, Hegerl GC, Schriever D, von Storch H, Zorita E (1997) A description of a 1260-year control integration with the coupled ECHAM1/LSG general circulation model. J Clim 10: 1525–1543
Zorita E, Frankignoul C (1997) Modes of North Atlantic decadal variability in the ECHAM1/LSG coupled ocean-atmosphere general circulation model. J Clim 10: 183–200